Design and characterization of cement-based materials for dihy-drogen trapping

Celine Cau Dit Coumes, Oriane Farcy, Jean-Baptiste Champenois, Pascal Antonucci, Adel Mesbah, David Lambertin

Design and characterization of cement-based materials for dihydrogen trapping

Céline Cau Dit Coumes[1], Oriane Farcy[1], Jean-Baptiste Champenois[1], Pascal Antonucci[1], Adel Mesbah[2], David Lambertin[1]

[1] CEA, DES, ISEC, DE2D, SEAD, Univ. Montpellier, Marcoule, France
[2] Univ. Lyon, Université Lyon 1, Institut de Recherches sur la Catalyse et l'Environnement de Lyon, IRCELYON, UMR5256, CNRS, Villeurbanne, France

* Corresponding Author, E-mail: celine.cau-dit-coumes@cea.fr

KEYWORDS: Dihydrogen, getter, magnesium phosphate cement, calcium sulfoaluminate cement, corrosion, radiolysis

1. Introduction

Mitigating the release of dihydrogen (H_2) is an important issue for the disposal of certain types of cemented waste packages, containing for instance metallic waste (such as aluminium, magnesium, uranium…) or highly irradiating waste. The dihydrogen production results from corrosion of the metals encapsulated in the cement matrix, and/or radiolysis of water. CEA has been working for several years on the sequestration of dihydrogen using an oxide getter of the γ-MnO_2/Ag_2O type [1]. This getter shows several advantages: reasonable cost due to the replacement of noble metals (Pd, Pt…) by Ag_2O as a promoter, good resistance to irradiation and irreversible trapping of H_2. The MnO_2/Ag_2O getter was first described by Kozawa *et al.* in the 1980s [2, 3, 4]. The allotropic form of MnO_2 strongly influences the H_2 trapping rate. The γ-MnO_2 phase (nsutite) made from an inter-growth of ramsdellite and pyrolusite was found to be the most efficient getter towards dihydrogen [1].The trapping mechanism was largely debated [5, 6], but recent work by Galliez *et al.* [7] using Fourier Transform Infra-Red (FTIR) spectroscopy and X-ray diffraction (Pair Distribution Function analysis) provided evidence of MnOOH formation in the allotropic forms of groutite (H in 2x1 tunnels) at first, and then of manganite (H in 1x1 tunnels). Analysis of the silver-based phase of the getter before trapping showed the presence of silver carbonate Ag_2CO_3 due to carbonation of Ag_2O during preparation of the getter. This presence of Ag_2CO_3 had a positive effect since it increased the sequestration rate of dihydrogen [8].

Self-levelling mortars, incorporating the getter, were designed with a view of their practical implementation as conditioning matrices for wastes leading to problematic dihydrogen release [9, 10]. Several authors showed that the efficiency of the getter decreases under wet environment [4, 9, 11,]. Thus, binders with a high chemical water demand, making it possible to obtain significant desaturation of the pore network by the sole hydration reactions, were selected to design the mortars. The study was focussed on two cements producing water-rich hydrates: a calcium sulfoaluminate (CSA) cement producing high contents of ettringite ($3CaO.Al_2O_3.3CaSO_4.32H_2O$), and a magnesium potassium phosphate (MKP) cement, mainly yielding K-struvite ($MgKPO_4.6H_2O$). The purpose was to investigate the chemical interactions occurring between the cement-based materials and the getter, and determine their influence on the performance of H_2 capture.

2. Materials and methods

2.1 Materials

The properties of the different raw materials used in this study are summarized in Table 1. Paste and mortar samples were prepared with a standardized mixer (EN 196-1) using the following sequence:

- pre-mixing of the dry products in a Turbula blender for 20 min,
- addition of the pre-mixed dry powders to the mixing water and mixing for 3 min at low speed.

Their composition is summarized in Tables 2 and 3.
The CSA cement comprised 20% anhydrite and 80% clinker with a high content of ye'elimite (54.3 wt.%). CSA cement-based materials exhibited a water-to-cement (w/c) ratio of 0.6. The MKP cement comprised magnesium oxide and potassium dihydrogen phosphate in equimolar amounts. All MKP-based

materials comprised fly ash at a fly ash-to-cement ratio of 0.8. This mineral addition improved both the rheological properties in the fresh state and the volume stability in the hardened state. Their water-to-cement ratio was set to 0.51, which corresponded to the amount of water theoretically required to precipitate K-struvite following equation (Eq. 1).

$$MgO + KH_2PO_4 + 5\ H_2O \rightarrow MgKPO_4.6H_2O \quad \text{(Eq. 1)}$$

Table 1: Raw materials.

Constituent	Supplier	Properties
Magnesium oxide, MgO Magchem 10CR	M.A.F. Magnesite	Calcined at high temperature (1300-1400°C) d_{10}=4.8 µm, d_{50}=18.9 µm, d_{90}=45.6 µm Specific surface area = 0.9 m²/g
Potassium dihydrogen phosphate, KH_2PO_4	Yara	Purity > 98% d_{10}=139 µm, d_{50}=303 µm, d_{90}=566 µm
Calcium sulfoaluminate clinker	Vicat Alpenat ^{UP}	d_{10}=3.3 µm, d_{50}=12.0 µm, d_{90}=42.4 µm Blaine surface area = 4650 cm²/g SiO_2 (10.55%), Al_2O_3 (23.46%), Fe_2O_3 (9.70%), CaO (45.07%), MgO (1.00%), TiO_2 (1.29%), Mn_2O_3 (0.01%), P_2O_5 (0.11%), SrO (0.06%), Na_2O 0.17%, K_2O 0.27%, SO_3 8.07%, Cl (0.01%), LOI 0.23%
Anhydrite	Vicat	d_{10}=4.8 µm, d_{50}=18.9 µm, d_{90}=70.6 µm $CaSO_4$ (85.0%), $CaSO_4.2H_2O$ (6.2%), $MgCO_3$ (4.7%), $CaMg(CO_3)_2$ (4.1 %)
Fly ash	Carling power station, France	d_{10}=3.0 µm, d_{50}=24.2 µm, d_{90}=136.1 µm Specific surface area = 2.2 m²/g MgO (2.15%), Al_2O_3 (25.75%), SiO_2 (50.30%), CaO (6.58%), Fe_2O_3 (5.92%), TiO_2 (1.36%), MnO (0.08%), P_2O_5 (0.67%), SrO (0.27%), Na_2O (0.78%), K_2O (1.53%), SO_3 (0.80%)
Boric acid $B(OH)_3$	VWR	Analytical grade (purity >99.5%)
Siliceous sand	Sibelco – Mios quarry	Grain size = 0.1-1.2 mm
	Leucate	Grain Size = 0-2 mm
Filler	Calcitec 2002 M	d_{10} = 2.6 µm, d_{50} = 13.6 µm, d_{90} = 40.5 µm $CaCO_3$ (98.86 wt%), MgO (0.21 wt.%), SiO_2 (0.16 wt.%), Al_2O_3 (0.05 wt%), Fe_2O_3 (0.03 wt.%), S (0.03 wt%)
Superplasticizer	BASF MasterEase 3000	-
γ-MnO_2	Merck ($Mn(IV)O_2$ precipitated active for synthesis)	d_{10} = 8.6 µm, d_{50} = 20.9 µm, d_{90} = 46.3 µm Specific surface area = 77 m²/g
γ-MnO_2/Ag_2O getter	A^3i	d_{10}=6.3 µm, d_{50}=20.4 µm, d_{90}=43.7 µm Specific surface area = 64.2 m²/g

Table 2: Calcium sulfoaluminate cement-based paste and mortar compositions (masses in g) (for 1 L).

Ref.	Clinker	Anhydrite	Water	Getter	γ-MnO_2	Leucate sand	Superplasticizer	Boric acid	Filler
CSA-P-G0	857.3	214.3	643.0	0	0	0	0	0	0
CSA-P-G5	842.2	210.5	631.6	88.7	0	0	0	0	0
CSA-P-G10	826.0	206.5	619.5	183.6	0	0	0	0	0
CSA-P-G15	808.6	202.2	606.5	285.4	0	0	0	0	0
CSA-P-NS10	826.0	206.5	619.5	0	183.6	0	0	0	0
CSA-M-G9.6	396.1	98.8	298.4	223.5	0	1156.5	2.5	7.4	130.7
CSA-M-NS9.6	396.1	98.8	298.4	0	223.5	1156.5	2.5	7.4	130.7

CSA = calcium sulfoaluminate cement; P = paste; M = mortar; Gx = getter at a mass content of x%, NSx = nsutite (γ-MnO_2) at a mass content of x%

Table 3: Magnesium phosphate cement-based paste and mortar compositions (masses in g) (for 1 L).

Ref.	MgO	KH_2PO_4	Sibleco sand	Fly ash	$B(OH)_3$	Water	Getter	γ-MnO_2
MKP-P-G0	177.6	599.5	0	621.7	31.1	396.3	0	0
MKP-P-G5	174.2	588.3	0	610.0	30.5	388.9	94.3	0
MKP-P-G10	170.7	576.2	0	597.5	29.9	380.9	195.0	0
MKP-M-G10	131.5	443.8	575.3	460.2	23.0	293.4	214.1	0
MKP-M-NS10	131.5	443.8	575.3	460.2	23.0	293.4	0	214.1

MKP = magnesium phosphate cement; P = paste; M = mortar; Gx = getter at a mass content of x%, NSx = nsutite (γ-MnO_2) at a mass content of x%

Boric acid was used as a retarder in CSA mortars and MPC materials at dosages of 1.5 % and 4 % (with respect to the weight of cement) respectively. It was dissolved in the mixing water at room temperature prior to mixing.
The getter content varied from 0 wt.% to 15 wt.% depending on the materials. Some reference pastes or mortars were also prepared by replacing the getter by pure nsutite (γ-MnO_2), which had almost the same particle size distribution as the getter but no sequestration properties of dihydrogen in the absence of the silver promoter.

2.2 Characterizations

Hydration of CSA and MPC cements was investigated using a TAM AIR conduction microcalorimeter under isothermal conditions at 25°C. About 2 g of paste were cast in a glass ampoule and introduced in the calorimeter. The heat flow was recorded versus time and compared to that of a sample maintained at 25°C and consisting of water, the volume of which being adjusted to get the same calorific capacity as the paste sample.

Cement hydration was stopped after fixed periods of time. The paste samples were ground in isopropanol and the suspensions were filtrated under vacuum at 0.45 µm. The solid fractions were gently dried for a minimum of 7 days in a controlled humidity chamber (with a 23% relative humidity at 22 ± 2°C controlled by a saturated solution of potassium acetate) and ground by hand to a particle size less than 100 µm before their characterization. Their mineralogy was investigated by powder X-ray diffraction with the Bragg Brentano geometry (PanAlytical X'pert Pro, copper anode, $\lambda_{K\alpha1}$=1.5418 Å, scanning from 2θ =5° to 120° in 0.017° steps, for a total counting time of 3h).

Thermogravimetric analyses were also carried out using a TGA/DSC Netzsch STA 409 PC instrument. The samples were heated under nitrogen (gas flow set at 50 mL/min) at 10°C/min up to 1000°C. The curves were corrected from buoyancy effects by performing a blank subtraction.

2.3 Titration of γ-MnO_2

Titration experiments were carried out to investigate the surface reactivity of γ-MnO_2 as a function of pH. Nsutite was suspended into demineralized water at a liquid-to-solid ratio varying from 50 mL/g to 400 mL/g depending on the trials. The titration reactor was tightly sealed and thermostated at 25° ± 0.5 °C by circulation of water in its double jacket. Suspensions were maintained under magnetic stirring and titrated with a 10 mmol/L NaOH solution using an automatic titrator (809 Titrando from Metrohm) controlled by Tiamo 2.1 software and equipped with a pH sensor calibrated using IUPAC pH buffers at 6.86, 9.18 and 12.45 (25°C). The equilibration time between two NaOH additions varied between 120 s and 3600 s. The volume increment of NaOH solution remained comprised between 10 µL and 50 µL.

2.4 Hydrogen sequestration

To assess the H_2-capture performance of the getter in cementitious environment, H_2 was produced *in situ* by encapsulating aluminum metal within MKP and CSA cement-based mortars containing either the getter (MKP-M-G10 and CSA-M-G9.6) or pure γ-MnO_2 (MKP-M-NS10 and CSA-M-NS9.6). In contact

with the pore solution, aluminum is corroded with production of dihydrogen [12]. The MKP and CSA mortars investigated in this work had a pore solution pH close to 8 and 12 respectively [9]. The corrosion rate of Al metal, which strongly depends on pH, was expected to be much smaller in the MKP matrix (where precipitation of alumina could passivate the metal) than in the CSA matrix (where aluminum was oxidized into soluble aluminate ions). The surface area of Al metal encapsulated in MKP and CSA mortars was thus adjusted in order to get significant production of H_2 in both cases. A high-purity (99.99%) aluminum rod (9.5 mm in diameter, 25 mm in length, surface area of 8.8 cm^2) was embedded into 100 mL of fresh CSA mortar while metallic powder (surface area of 8680 cm^2) was dispersed into 100 mL of MKP mortar during mixing. The fresh samples, poured in polyethylene cells, were then placed in metal reactors with a cover tap that could be connected to a vacuum pump, to a nitrogen supply, or to a gas chromatograph (Figure 1). The reactors were hermetically sealed. They were placed under vacuum at a pressure of 150 mbar before filling with nitrogen up to a pressure of 750 mbar. The reactors were stored at room temperature (22 ± 2°C) and gas samples were taken at regular intervals for hydrogen analysis by gas chromatography (Varian 3400, argon carrier gas, capillary column, thermal conductivity detector, detection limit corresponding to 0.01% hydrogen in the reactor headspace).

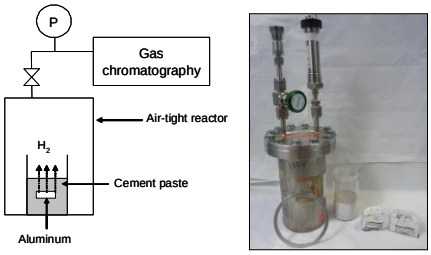

Figure 1: Device for measuring the hydrogen released from mortar samples encapsulating Al metal.

2.5 Thermodynamic modelling

ProtoFit software [13] was used to analyze acid/base titration data and optimize surface protonation models : the protonation constants of the different surface sites were estimated by calculating an adsorbent proton buffering function from raw titration data, and by minimizing the weighted sum of squares between this function and the model prediction.
Chess software [14] and the Minteq thermodynamic database [15] which contained relevant silver minerals and aqueous species were used to investigate the thermodynamic stability of silver carbonate as a function of pH and $CaSO_4$ or KH_2PO_4 concentrations.

3. Results and discussion

3.1 Influence of the getter on MKP and CSA cement hydration

The fraction of bound water in MKP and CSA cement pastes comprising 0 wt% or 10 wt% getter was assessed as a function of time using the weight loss recorded by TGA from 25°C to 400°C (Figure 2).

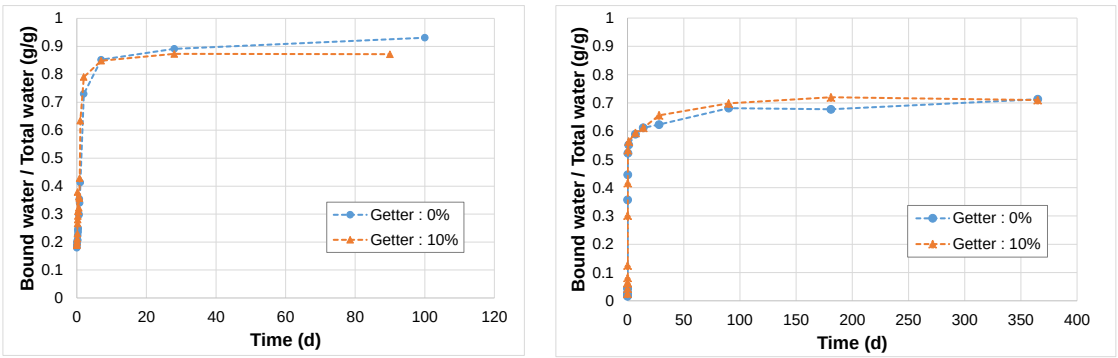

Figure 2: Influence of the getter content on the evolution of the fraction of bound water as a function of time. Left: paste samples MKP-P-G0 and MKP-P-G10, right: paste samples CSA-P-G0 and CSA-P-G10.

The fraction of bound water reached a higher plateau value in MKP cement pastes (~90 %) than in CSA cement pastes (~70 %) and did not depend on the getter content. Note that the initial bound water content in the MKP pastes had a non-zero value because some water was bound in the reactants KH_2PO_4 and $B(OH)_3$.
Similarly, comparing the X-ray diffraction patterns of hardened cement pastes having reached significant hydration degree showed that the getter content had no influence on the mineralogical assemblages (Figure 3). MKP cement pastes mainly comprised K-struvite, with small amounts of residual magnesium oxide, and quartz originating from fly ash. The getter, which was poorly crystallized, was not evidenced by X-ray diffraction. CSA cement pastes contained hydrated phases (ettringite, monosulfate and strätlingite), as well as residual minerals from cement (dicalcium silicate, traces of anhydrite, and non-reactive perovskite and merwinite).

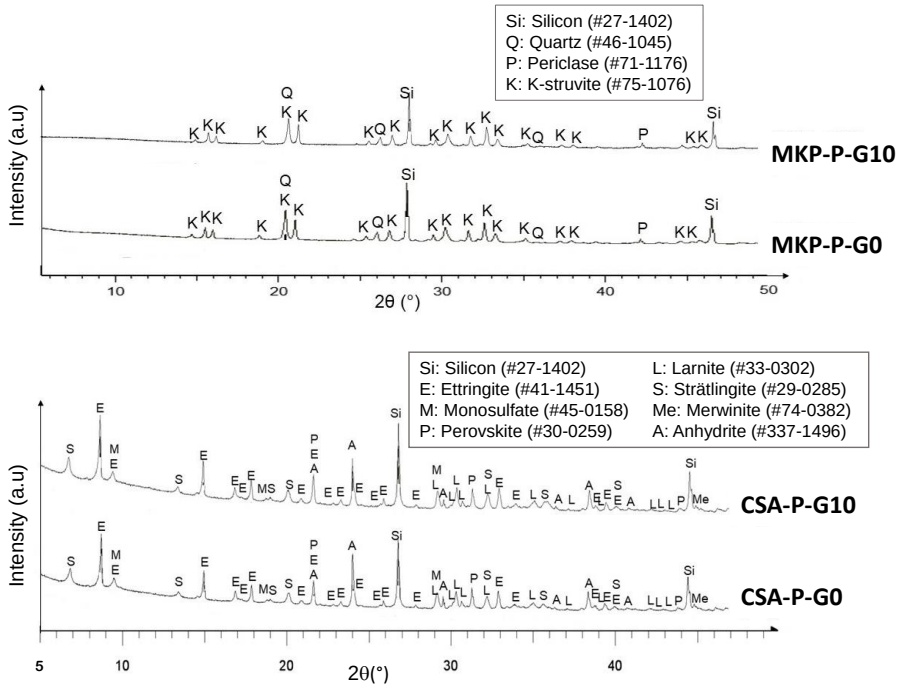

Figure 3: Influence of the getter content on the phase assemblage of hardened cement pastes cured at 20°C under endogenous conditions. Top: MKP-P-G0 and MKP-P-G10 paste samples cured for 28 d, right: CSA-P-G0 and CSA-P-G10 paste samples cured for 180 d. Silicon is used as an internal standard.

Isothermal conduction calorimetry was used to investigate hydration of cement pastes at early age. The heat flow curves are shown in Figure 4. The first minutes were characterized by heat production which resulted from several factors: start of dissolution of cement anhydrous phases (MgO or ye'elimite), but also introduction of the externally prepared sample in the calorimetric chamber, which biased the signal. The heat flow produced by the different cement pastes was thus recorded from 30 minutes onwards. Two heat flow peaks were evidenced, indicating that hydration occurred in several steps. In the case of MKP cement pastes, the peaks were attributed to dissolution of MgO (the main exothermic process) leading to the precipitation of an amorphous transient product (first peak), and then to K-struvite (second peak) [9]. Regarding CSA cement pastes, Winnefeld *et al*. [16] reported that the first peak was due to massive consumption of ye'elimite to form ettringite and aluminum hydroxide, and the second one was caused by the depletion of sulfate and calcium ions from the solution, leading to additional precipitation of monosulfate. The getter seemed to influence the early stages of hydration of both cements. Increasing its content accelerated MKP cement hydration, the two heat flow peaks being recorded after shorter periods of time. Reversely, the first heat flow peak of CSA cement pastes was slightly delayed and its intensity decreased. A broadening of the second heat flow peak was also observed, indicating that the getter weakly retarded CSA cement hydration at early age. Given the high specific surface area of the getter, acceleration of MKP cement hydration could result from a filler effect. Explaining the retardation of CSA cement would deserve complementary characterization to analyze the evolution of the pore solution composition with and without any getter. For both cements however, the heat flow recorded initially, from 30 minutes to 1 h, seemed to

increase with the getter content, suggesting the occurrence of an exothermic process involving the getter shortly after mixing. Additional experiments were thus carried out to investigate the getter reactivity in synthetic solutions mimicking the pore solution of the materials.

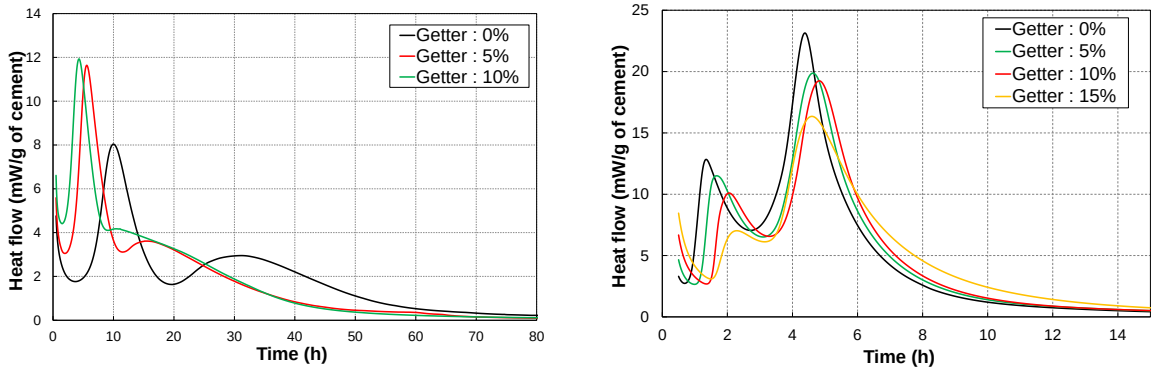

Figure 4: Heat flow produced by MKP (left –MKP-P-G0, MKP-P-G5 and MKP-P-G10 samples) and CSA cement pastes (right – CSA-P-G0, CSA-P-G5, CSA-P-G10 and CSA-P-G15 samples).

3.2 Getter reactivity in simplified synthetic pore solutions

The getter comprised 85% γ-MnO_2 and 15% Ag_2CO_3. The reactivity of these two components was investigated in simplified cementitious environments.

3.2.1 Ag_2CO_3

Stability of Ag_2CO_3 was studied using thermodynamic modelling. The temperature and the initial Ag_2CO_3 concentration were set to 25°C and 10 mmol/L respectively. The solution pH was adjusted by adding HNO_3 or NaOH to the system. Figure 5 shows the evolution of silver minerals as a function of pH in the presence of potassium phosphate or calcium sulfate. In MKP cement pastes, the pore solution pH evolves from 4 to 8 with ongoing hydration [17]. Figure 5 (left) indicates that silver carbonate is not stable in the initial acidic mixing solution and should thus dissolve. Besides, in the presence of phosphates, silver phosphate should predominate over silver carbonate in the pH range relevant to the hardened material. In CSA cement pastes, the pore solution pH, initially neutral, is rapidly raised to a value which remains close to 11 as long as anhydrite is present [18]. According to Figure 5 (right), silver carbonate is destabilized at the expense of silver oxide at high pH. Moreover, the stability domain of silver carbonate is reduced in the presence of calcium sulfate since carbonate ions tend to precipitate as calcite. These calculations thus show that in both kinds of cement pastes, silver carbonate, the promoter of the getter, should evolve from a thermodynamic point of view.

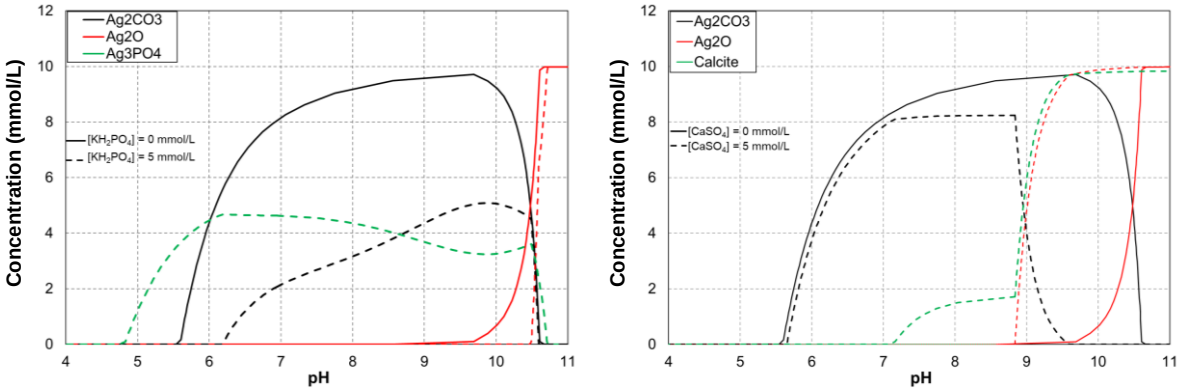

Figure 5: Thermodynamic investigation of Ag_2CO_3 stability as a function of pH in the presence or absence of KH_2PO_4 (left) or $CaSO_4$ (right).

3.2.2 γ-MnO_2

A suspension of γ-MnO_2 (the main component of the getter) in demineralized water was titrated with sodium hydroxide. The titration curve, shown in Figure 6, strongly deviated from the theoretical curve

calculated assuming inert γ-MnO_2. Since γ-MnO_2 is highly insoluble over the investigated pH range [19] and no secondary phase was evidenced by X-ray diffraction, the deviation likely resulted from surface hydroxylation of γ-MnO_2, a process already reported for other polymorphs such as δ-MnO_2 [20].

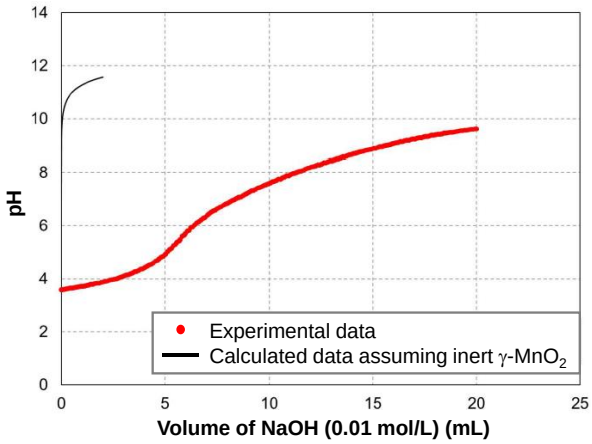

Figure 6: Titration of a suspension of nsutite in demineralized water by sodium hydroxide (0.01 mol/L) (Liquid/solid ratio = 50 mL/g, volume of water = 20 mL, mass of nsutite = 400 mg).

Two models were tested to describe the surface chemistry of γ-MnO_2 as a function of pH (Figure 7). The first one assumed a homogeneous surface consisting of equivalent amphoteric binding sites, whereas the second one considered a heterogeneous surface with two non-equivalent classes of binding sites (one class of amphoteric sites, and one class of acidic sites which could deprotonate). In both cases, the electrostatic contribution was described using the diffuse layer model [21], which was selected for its simplicity. The model parameters were determined experimentally (specific surface area of nsutite) or adjusted (intrinsic formation constants, site density) using ProtoFit software in order to fit a set of titration curves of γ-MnO_2 suspensions with different liquid/solid ratios.

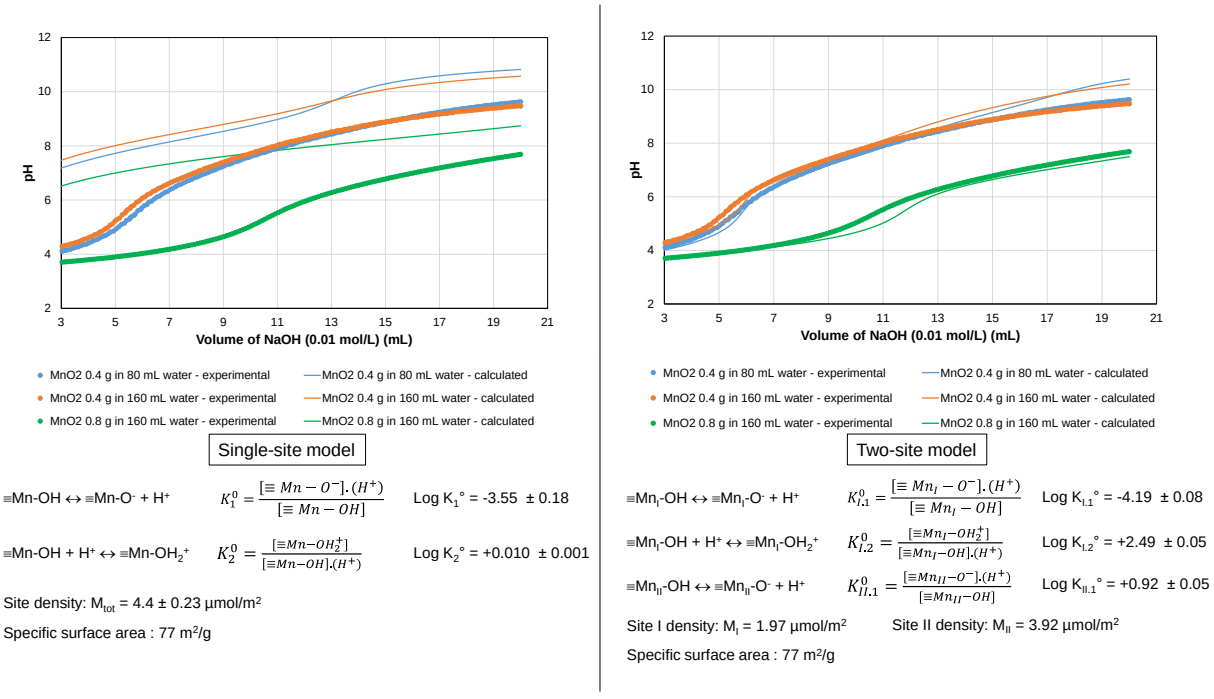

Figure 7: Models tested to describe the surface reactivity of γ-MnO_2: single-site model (left) and two-site model (right) – Comparison of calculated and experimental titration curves of γ-MnO_2 by NaOH 0.01 mol/L (T = 25°C, P = 1 atm)

The single-site model failed to reproduce the experimental data. Significant improvement was provided by the two-site model. A deviation between calculated and experimental data persisted however in some

cases at high pH (> 9), possibly because sorption of sodium ions was neglected in this first modelling approach. The densities of the two site classes differed by a factor 2. Two assumptions were postulated to explain the surface heterogeneity. *(i)* From a structural point of view, nsutite is made from an inter-growth of ramsdellite and pyrolusite and comprises 1x1 and 2x1 channels. Galliez [22] quantified the fractions of 1x1 channels (from pyrolusite) and 2x1 channels (from ramsdellite) in a sample of nsutite provided by the same supplier as in this study and obtained a ratio of 1.94 close to that of the site densities, suggesting that the two site classes might be associated with the two types of channels. *(ii)* The occurrence of manganese at two oxidation states (+IV, and +III) was the second hypothesis. It could account for the significantly different pK_a values of the two site classes.
Using the two-site model, it was possible to plot the evolution of the different surface site fractions as a function of pH (Figure 8). Extrapolating to zero the curve showing the net surface charge (Q) led to a point of zero charge (pzc) close to pH 2.6. In the range of pH values relevant to MKP (4-8) and CSA (7-12) cement pastes, the net surface charge of γ-MnO_2 was thus negative, despite the occurrence of positively charged Mn_I-OH_2^+ sites up to pH 9. The higher the pH, the stronger the negative charge. Sorption of ions, and especially of cations, onto γ-MnO_2 surface of was thus likely.

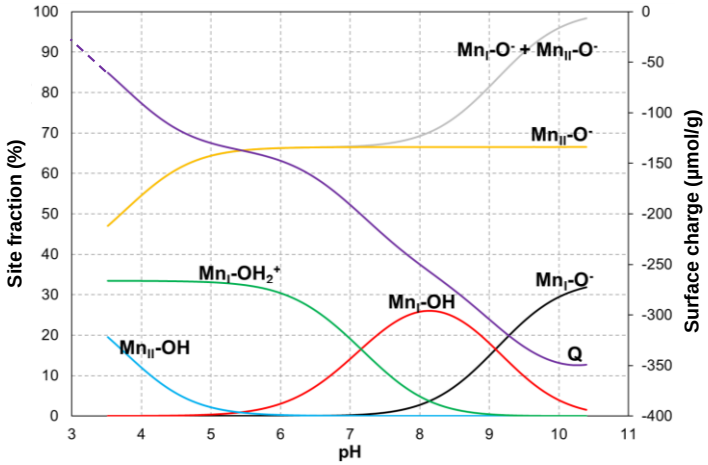

Figure 8: Speciation of γ-MnO_2 surface sites as a function of pH calculated using the two-site model (Q stands for the net charge of the surface).

Based on these results, an explanation to the heat flow increase of cement pastes containing the getter during their early stage of hydration (up to 1 h – see Figure 4) could be proposed. Initial dissolution of the anhydrous cement phases would tend to be accelerated due to consumption of some ions released in solution which sorbed onto γ-MnO_2 (especially Ca^{2+}, K^+ and Mg^{2+}), pH variation and/or precipitated with silver (phosphate and hydroxide ions) or carbonate (Ca^{2+}).

3.3 Sequestration of dihydrogen produced by corrosion of Al metal encapsulated in MKP and CSA cement-based mortars

In the previous section, it was shown that the getter could react in a cementitious environment: the negatively charged surface of γ-MnO_2 likely sorbed cations while silver carbonate was, at least partly, destabilized into silver phosphate (MKP material) or silver oxide (CSA material). This raised the following question: did the getter keep its efficiency to capture dihydrogen despite its chemical evolution?
Some metallic aluminium (powder or rod) was encapsulated in MKP- and CSA-cement based mortars containing either the getter (MKP-M-G10 and CSA-M-G9.6) or pure γ-MnO_2 (MKP-M-NS10 and CSA-M-NS9.6) which, in the absence of any promoter, lost its ability to capture dihydrogen. The hydrogen released from the different materials was analysed by gas chromatography and plotted versus the time of curing (Figure 9).

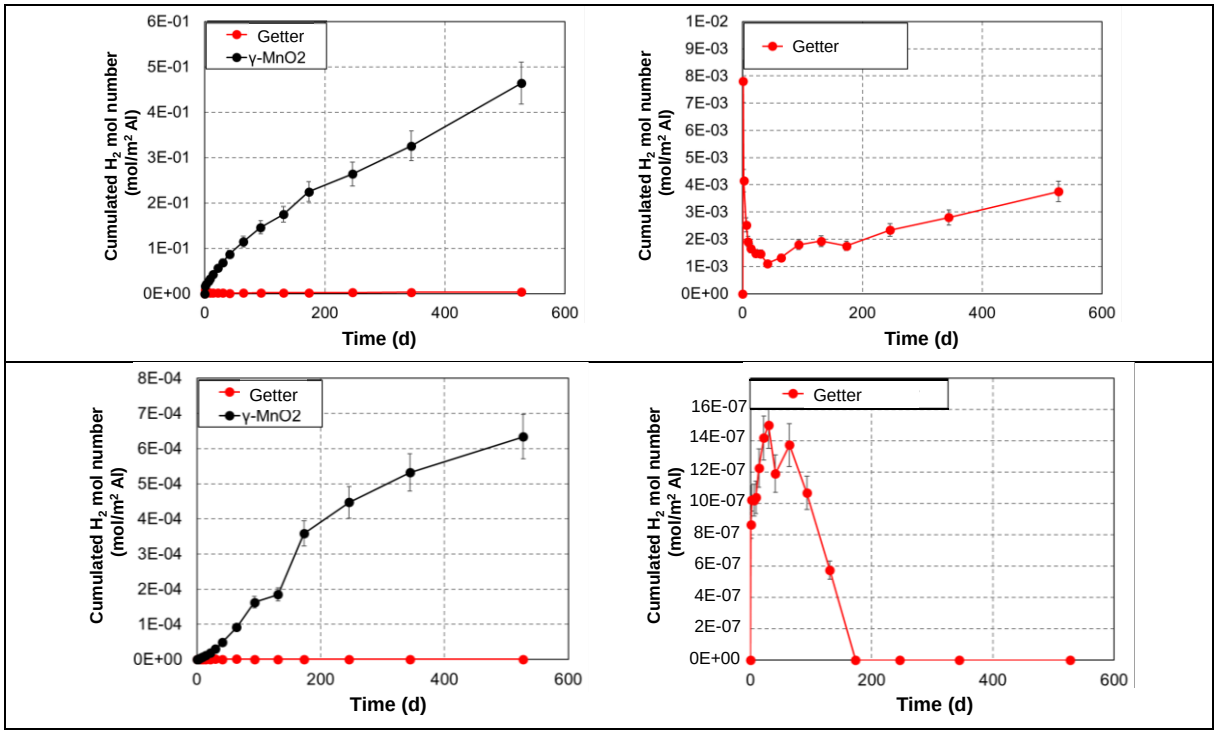

Figure 9: Cumulated mol number of dihydrogen released by CSA (top) or MKP cement-based mortars (bottom) containing ~10 wt.% getter or γ-MnO_2.

Regardless of the type of cement used, the amount of dihydrogen released by the mortars was much smaller in the presence of getter. After one year of curing, it was divided by a factor 73 and 1266 in CSA and MKP mortars respectively. The getter also led to non-monotonous release of dihydrogen. A first concentration peak was observed after 1 d in the headspace of the reactor containing the CSA cement-based mortar. The H_2 content then decreased up to 41 d, before increasing again afterwards, but more slowly. Cau Dit Coumes *et al*. [12] have already shown that the H_2 production resulting from Al corrosion in a CSA cement paste is rapid during the first day after mixing, then slows down due to consumption of water by ongoing hydration, and accelerates again after 50 d. This acceleration is linked to the depletion of calcium sulfate from the system, which leads to a pore solution pH rise by about one unit, and thus promotes corrosion of Al metal. In CSA-M-G9.6 mortar, the H_2 trapping rate by the getter was not high enough to avoid the initial release. The subsequent decrease in the H_2 gaseous concentration could be explained by delayed capture of the initial gas pulse. Finally, the corrosion rate of aluminium accelerated due to pH increase and a slow H_2 release occurred again. Regarding MKP-M-G10 mortar, H_2 was released in small amounts in the headspace of the reactor up to 64 d. Its content then decreased and remained constant after 173 d, meaning that a stationary state was reached.

The fraction of H_2 captured by the getter was estimated by comparing, for a given binder, the H_2 release with the getter and with γ-MnO_2 (reference). It increased with time and reached 99.0% and 99.9 % in CSA and MKP mortars respectively (Figure 10).

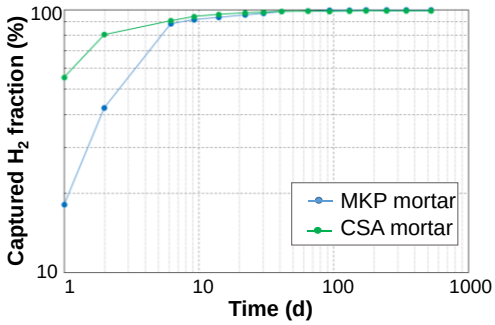

Figure 10: Comparison of the fractions of dihydrogen trapped by CSA-M-G9.6 and MKP-M-G10 mortars.

This increase could result from progressive auto-desiccation of the mortars. The H_2 production rate decreased since hydration consumed water. Meanwhile, the getter trapping efficiency increased in dryer environment. Finally, it was checked that the amount of H_2 captured after 18 months of curing (2.5×10^{-5} mol/g of getter in MKP-M-G10 mortar, 2.1×10^{-5} mol/g of getter in CSA-M-G9.6 mortar) remained much smaller than the trapping capacity of the as-supplied getter (5.7 mmol H_2/g).

4. Conclusion

The main conclusions of this work can be summarized as follows.

1. The getter slightly influenced cement hydration at early age (acceleration of MKP cement, retardation of CSA cement), but had no effect at later age. In particular, the bound water content and phase assemblage of hardened cement pastes remained unchanged.
2. The getter was not inert in cementitious environment. Based on thermodynamic calculations, silver carbonate should destabilize at the expense of silver phosphate in the MPC matrix, while precipitations of silver oxide and calcite were expected in the CSA matrix. Surface reactivity of γ-MnO_2 was also evidenced, making it possible to sorb ions released by the dissolution of cement phases. A two-site model was built to describe the ionization of the γ-MnO_2 surface. In the pH range relevant for cementitious materials, the net surface charge remained negative.
3. Despite its evolution in the cement-based materials, the getter still enabled to capture significant amounts of dihydrogen. The H_2 release of mortars encapsulating aluminium metal was strongly mitigated, especially when MKP cement was used. This result offers new prospects to optimize the conditioning of reactive metals in cement matrices.

5. Acknowledgements

This work was supported by Andra as part of the program “Investissements d’Avenir” funded by the French government.

6. References

[1] K. Galliez, P. Deniard, D. Lambertin, S. Jobic, F. Bart, Influence of MnO_2 polymorphism form on MnO_2/Ag_2O hydrogen getter, J. Nucl. Mater. 438 (2013) 261-267

[2] A. Kozawa, Reaction mechanism of hydrogen absorbers made of manganese dioxide, Denki Kagaku 44 (1976) 572-577

[3] A. Kozawa, Hydrogen Gas Absorber Made of MnO_2 Catalysed with Palladium or Platinium Salts, Denki Kagaku 46 (1978) 416-418

[4] A. Kozawa, K.V. Kordesch, Silver-catalysed MnO_2 as hydrogen absorber, Electrochimica Acta 26 (1981) 1489-1493

[5] C. Maruéjouls, E. Bachellerie, C. Latgé, A. Laurent, J.M. Le Lann, J.C. Robin, S. Rosenvallon, Mitigation of the hydrogen risk in fusion facilities: the first experimental results, Fusion Engin. Design 69 (2003) 585-591

[6] Y. Chabre, J. Pannetier, Structural and electrochemical properties of the proton /ɣ-MnO_2 system, Progress Solid State Chem. 23 (1995) 1-130

[7] K. Galliez., P. Deniard, C. Payen, D. Lambertin, F. Bart, H.J. Koo, M.H. Whangbo, S. Jobic, Pair Distribution Function and Density Functional Theory Analyses of Hydrogen Trapping by γ-MnO_2, Inorg. Chem. 54 (2015) 1194-1196

[8] K. Galliez, P. Deniard, P.E. Petit, D. Lambertin, F. Bart, S. Jobic, Modelling and quantification of intergrowth in gamma-MnO_2 by laboratory pair distribution function analysis, J. Applied. Cryst. 47 (2014) 552-560

[9] A. Farcy, Formulation et caractérisation de mortiers fluides pour le conditionnement de déchets tritiés, Thèse de doctorat l’Université de Montpellier (2020) (in French)

[10] S. Lanier, Mise au point d’un mortier de piégeage à réseau poreux contrôlé, Thèse de doctorat de l’Ecole Centrale de Lille (2020) (in French)

[11] V. Chaudron, Etude de la mitigation du risque hydrogène dans un réacteur de fusion thermonucléaire par réduction d’un oxyde métallique, Thèse de Doctorat de l’Institut National Polytechnique de Lorraine (1988) (in French)

[12] C. Cau Dit Coumes, D. Lambertin, H. Lahalle, P. Antonucci, C. Cannes, S. Delpech, Selection of a mineral binder with potentialities for the stabilization / solidification of aluminum metal, J. Nucl. Mater. 453 (2014) 31-40

[13] B. F. Turner, J. B. Fein, ProtoFit: A program for determining surface protonation constants from titration data, Computers & Geosciences 32 (2006) 1344–1356

[14] J. Van Der Lee, Thermodynamic and Mathematical Concepts of CHESS, Technical report LHM/RD/98/39 (1998) LHM/RD/98/39.

[15] L.E. Eary, E.A. Jenne, Version 4.0 of the Minteq Geochemical Code, PNL 8190 DE 93 000968 (1992) 159 p

[16] F. Winnefeld, S. Barlag, Calorimetric and thermogravimetric study on the influence of calcium sulfate on the hydration of ye'elimite. J. Thermal Anal. Calorim. 101 (2010) 949-957

[17] H. Lahalle, Conditionnement de l'aluminium métallique dans les ciments phospho-magnésiens, Thèse de doctorat de l'Université de Bourgogne (2016) (in French)

[18] F. Winnefeld, B. Lothenbach, Hydration of calcium sulfoaluminate cements — Experimental findings and thermodynamic modelling, Cem. Concr. Res. 40 (2010) 1239–1247

[19] S. Parc, D. Nathon, Y. Tardy, P. Vieillard, Estimated solubility products and fields of stability for cryptomelane, nsutite, birnessite and lithiophorite based on natural lateritic weathering sequences, American Mineralogist 74 (1989) 466-475

[20] P.J. Pretorius, P.W. Linder, The adsorption characteristics of δ-manganese dioxide: a collection of diffuse double layer constants for the adsorption of H^+, Cu^{2+}, Ni^{2+}, Zn^{2+}, Cd^{2+} and Pb^{2+}, Applied Geochem. 16 (2001) 1067-1082

[21] W. Stumm, C.P. Huang, S.R. Jenkins, Specific chemical interaction affecting the stability of dispersed systems, Croatica Chemica Acta 42 (1970) 223-245

[22] K. Galliez, Etude et compréhension du piégeage irréversible de l'hydrogène à l'aide d'un mélange MnO_2/Ag_2O, Thèse de doctorat de l'Université de Nantes (2012) (in French)